

Double-Side Near-Field Channel Estimation for Extremely Large-Scale MIMO System

Yu Lu, *Student Member, IEEE*, and Linglong Dai, *Fellow, IEEE*

Abstract

Accurate channel estimation is essential to empower extremely large-scale MIMO (XL-MIMO) in 6G networks with ultra-high spectral efficiency. Unfortunately, most of the existing channel estimation methods designed for XL-MIMO fail to consider a *double-side near-field scenario*, where both transmitter and receiver are equipped with extremely large-scale antenna arrays. The existing channel estimation schemes cannot be directly applied to the double-side near-field scenario. In this paper, based on this scenario, we first derive double-side near-field Rayleigh distance (DS-RD) and effective double-side near-field Rayleigh distance (EDS-RD) to determine the range of the double-side near-field region. Then, a double-side near-field channel model is proposed to match this scenario, where the distance of the transmitter from the receiver is smaller than EDS-RD. In the proposed channel model, the line of sight (LoS) path component is modeled by the geometric free assumption while non-line of sight (NLoS) path components are modeled by the near-field array response vectors. Finally, a double-side near-field channel estimation algorithm is proposed to solve the channel estimation problem in this scenario, where the LoS path component and NLoS path components are estimated separately. Numerical simulation results demonstrate that, the proposed channel estimation algorithm is able to outperform the existing methods.

Index Terms

6G, extremely large-scale MIMO, channel estimation, double-side near-field.

All authors are with the Beijing National Research Center for Information Science and Technology (BNRist) as well as the Department of Electronic Engineering, Tsinghua University, Beijing 100084, P. R. China (e-mails: y-lu19@mails.tsinghua.edu.cn, daill@tsinghua.edu.cn).

This work was supported in part by the National Key Research and Development Program of China (Grant No.2020YFB1807201) and the National Natural Science Foundation of China (Grant No. 62031019)

I. INTRODUCTION

Due to the emergence of new applications such as digital twin, holographic imaging, and extended reality, the spectral efficiency of 6G is expected to grow tenfold [1]–[3]. To achieve higher spectral efficiency, the extremely large-scale MIMO (XL-MIMO) is regarded as one of the most important technology for 6G [4], [5]. In XL-MIMO communications, by exploiting the high spatial multiplexing gain, the transmitter equipped with an extremely large-scale antenna array serves multiple users to achieve better spectral efficiency.

In order to obtain spatial multiplexing gain, XL-MIMO should generate a directional beam with high array gain by beamforming. Before realizing beamforming, the channel state information (CSI) should be acquired in advance by channel estimation [6], [7]. Moreover, precise description of the transmission electromagnetic (EM) environment, or the channel model, is important for designing advanced channel estimation scheme. Accordingly, the fundamental EM property should be delicately analyzed for modeling and estimating the XL-MIMO channel [8].

A. *Prior Contributions*

The existing channel estimation methods for XL-MIMO can be divided into two categories, i.e., far-field channel estimation methods [9]–[12] and near-field channel estimation methods [13], [14]. For the far-field channel estimation, where the planar wave assumption is considered, the receiver of the XL-MIMO system is regarded to be located in the transmitter’s far-field region. There are three typical kinds of methods for far-field channel estimation, including statistical characteristics, spatial sparsity, and machine learning-based channel estimation. For statistical characteristics-based methods, the channel property can be modeled by channel correlation matrices, which are based on the distance of the transmitter from the receiver. The channel correlation matrices are usually low-rank and quasi-static. Therefore, the statistical characteristics-based channel estimation can use correlation matrices to obtain the high-dimensional channel in a long time [9]. For spatial sparsity-based channel estimation, the channel is modeled based on the far-field array response vector, which is only determined by angle due to the planar wave assumption. By utilizing the channel sparsity in angle-domain, some of the existing compressed sensing (CS) algorithms [10] are usually utilized to estimate this with channel low pilot overhead. Apart from the above two methods, machine learning is gaining popularity for channel estimation recently. In this category, some information of channel is usually exploited to reduce the complexity or improve the channel estimation accuracy [11], [12].

The second category for XL-MIMO channel estimation is near-field channel estimation, where the receiver is in the near-field region of the transmitter under the condition of spherical wave assumption. Specifically, due to the enlarged array aperture of XL-MIMO, the receiver is more likely to lie in the transmitter's near-field region, which is usually defined by the Rayleigh distance (RD) $Z = 2D^2/\lambda$ [15]. The RD is proportional to the square of the array aperture D^2 and the inverse of wavelength $\frac{1}{\lambda}$. Thus, it is obvious that the near-field region of the transmitter with an extremely large-scale antenna array expands by orders of magnitude as the array aperture becomes much larger. Considering the near-field effects, the XL-MIMO channel should be modeled to ensure accuracy in the near-field range under the condition of the spherical wave assumption [14], [16] instead of the planar wave assumption as far-field. For example, [13] considers the scenario where the transmitter employs an extremely large-scale antenna array serving multiple single-antenna receivers. In this scenario, the receivers are located in the transmitter's near-field region. Thus, channels between the transmitters and receivers are modeled based on a near-field array response vector, which relates not only to angle but also to the distance due to the spherical wave assumption. To estimate the near-field channel, the whole two-dimensional distance-angle plane is uniformly partitioned into multiple grids, and then the corresponding near-field transform matrix can be constructed by multiple near-field array response vectors associated with different grids. By means of the constructed transform matrix, the near-field channel shows sparsity in the transform domain, which can be estimated by CS-based methods with low pilot overhead. The authors of [14] also consider the same scenario as that in [13], interestingly, it is proved that the distance should be non-uniformly divided to reduce the correlation among the near-field array response vectors of the transform matrix in [14]. Based on the improved transform matrix, a new sparse representation in polar-domain is proposed in [14] for XL-MIMO. By utilizing this polar-domain sparsity, a CS-based algorithm has been proposed to raise the estimation accuracy.

Notice that all the existing near-field channel estimation schemes assume that the transmitter employs an extremely large-scale antenna array, while the receiver employs a single antenna. This model has caused that, the receiver is in the near-field region of the transmitter, while the transmitter is in the far-field of the receiver, i.e., “*single-side near-field (SS-NF)*”. However, in practice, the transmitter and receiver are likely to employ the extremely large-scale antenna arrays simultaneously. In this scenario, the transmitter and receiver may be in each other's near field region at the same time, i.e., “*double-side near-field (DS-NF)*”. For instance, in [17],

an extremely large-scale antenna array is installed on the top of a car, and the transmitter also deploys an extremely large-scale antenna array. In this case, when the transmitter and receiver are both in a near-field range, the existing single-side channel model based on a near-field array response vector will mismatch the XL-MIMO scenario in practice. Therefore, the existing near-field channel estimation schemes cannot estimate the XL-MIMO channel accurately. Unfortunately, there is no study of this important problem for XL-MIMO in the current literature.

B. Our Contributions

In order to solve this problem, a DS-NF channel estimation scheme is proposed based on the proposed accurate DS-NF XL-MIMO channel model. Our specific contributions are listed below.

- 1) In this paper, we first define the range of the DS-NF region. Specifically, similar to the derivation of RD, by considering the condition that the total maximum allowable phase error between the DS-NF channel and the far-field channel in the free space cannot exceed $\pi/8$, we first define the double-side near-field Rayleigh distance (DS-RD), which is proportional to the square of the sum of the antenna array aperture of the transmitter and receiver. Then, by considering the condition that the relative maximum allowable phase error between the DS-NF channel and the SS-NF channel in the free space is no more than $\pi/8$, the effective double-side near-field Rayleigh distance (EDS-RD) is calculated, which is proportional to the product of the transmitter and receiver array apertures.
- 2) By considering the defined EDS-RD, we propose a DS-NF channel model to match the DS-NF scenario, where the distance of the transmitter from the receiver is smaller than EDS-RD. Specifically, the NLoS path components and LoS path component are modeled separately. NLoS path components are modeled based on the near-field array response vector, which is similar to the far-field channel model based on the far-field array response vector. By contrast, the LoS path component is modeled based on the precise geometric free space assumption.
- 3) Based on the proposed DS-NF channel model, the corresponding DS-NF channel estimation algorithm is proposed to estimate the XL-MIMO channel accurately. In our proposed DS-NF channel estimation algorithm, the LoS and NLoS path components are estimated separately. The LoS path component is estimated by hierarchical parameter estimation, while the NLoS path components are estimated by orthogonal matching pursuit (OMP)-

based estimation with their polar-domain sparsity. We provide numerical simulation results to illustrate the effectiveness of our scheme.

C. Organization and Notation

Organization: The rest of the paper is organized as follows. In Section II, the signal model and current far-field XL-MIMO and SS-NF XL-MIMO channel models are introduced. Then, the DS-RD and EDS-RD are derived to determine the range of the DS-NF region. In Section III, In Section IV, we propose the DS-NF channel model. In Section V, we propose the corresponding channel estimation scheme based on the proposed DS-NF channel model. Simulation results is provided in Section VI, and finally, conclusions is provided in Section VII.

Notation: Lower-case and upper-case boldface letters \mathbf{a} and \mathbf{A} denote a vector and a matrix, respectively; $\|\mathbf{A}\|_F$ denotes the Frobenius norm; \mathbf{a}^H and \mathbf{A}^H denote the conjugate transpose of vector \mathbf{a} and matrix \mathbf{A} , respectively. The circularly symmetric complex Gaussian distribution is denoted by $\mathcal{CN}(\mu, \sigma^2)$, with its mean set to μ and variance set to σ^2 , and $\mathcal{U}(-a, a)$ denotes the uniform distribution on $(-a, a)$. \otimes denotes the Kronecker product. \mathbf{I} denotes the identity matrix.

II. SYSTEM MODEL

In this section, the signal model of the XL-MIMO system used in this paper will be introduced first. Then, we will review the existing far-field XL-MIMO and near-field XL-MIMO channel models.

A. Signal Model

In this work, we consider that the transmitter and receiver are equipped with N_1 -element and N_2 -element extremely large-scale antenna arrays, respectively. Let $\mathbf{H} \in \mathbb{C}^{N_2 \times N_1}$ denotes the channel from transmitter to receiver. The corresponding signal model can be presented as

$$\mathbf{Y} = \mathbf{H}\mathbf{P} + \mathbf{N}, \quad (1)$$

where $\mathbf{Y} \in \mathbb{C}^{N_2 \times M}$ and $\mathbf{P} \in \mathbb{C}^{N_1 \times M}$ denote the received pilots signal and the transmitted pilots signal in M times slots, and $\mathbf{N} \sim \mathcal{CN}(\mathbf{0}, \sigma^2 \mathbf{I}_{N_2} \otimes \mathbf{I}_M)$ denotes the $N_2 \times M$ received noise in M times slots with σ^2 representing the noise power. In channel estimation problem, we need to estimate \mathbf{H} with given \mathbf{P} and \mathbf{Y} . The number of transmitter and receiver antennas N_1 and N_2 is

large in the XL-MIMO system. Thus, to reduce the pilot overhead in a practical communication system, the channel estimation scheme with low overhead should be utilized, where the number of pilots M is much smaller than N_1 . Since the channel model is significant for designing a channel estimation scheme, we will review the current XL-MIMO channel models next.

B. Existing XL-MIMO Channel Models

The electromagnetic wave can propagate in two kinds of modes, i.e., far-field mode and near-field mode. As mentioned before, the boundary between these two modes is the RD. It is obvious that different modes of fields will lead to different channel models. The existing far-field channel model and near-field channel model are described as follows.

1) *Far-Field*: As mentioned in Subsection I-A, when the distance of the transmitter from the receiver is greater than the RD, by considering the planar wave assumption, the far-field MIMO channel $\mathbf{H}_{\text{far-field}}$ is modeled, which can be presented as [18]

$$\mathbf{H}_{\text{far-field}} = \sqrt{\frac{N_1 N_2}{L}} \sum_{l=1}^L \alpha_l \mathbf{a}(\theta_{l_{\text{AOA}}}) \mathbf{a}^H(\theta_{l_{\text{AOD}}}), \quad (2)$$

where L denotes the number of path components between the transmitter and the receiver, $\theta_{l_{\text{AOA}}}$ ($\theta_{l_{\text{AOD}}}$) and α_l denote the angle of arrival (departure) and gain for the l -th path. With the planar wave assumption, $\mathbf{a}(\theta_{l_{\text{AOA}}})$ and $\mathbf{a}(\theta_{l_{\text{AOD}}})$ represent the far-field array response vector, which is presented as

$$\begin{aligned} \mathbf{a}(\theta_{l_{\text{AOA}}}) &= \frac{1}{\sqrt{N_2}} \left[1, e^{-j\frac{2\pi}{\lambda}d\theta_{l_{\text{AOA}}}}, \dots, e^{-j(N-1)\frac{2\pi}{\lambda}d\theta_{l_{\text{AOA}}}} \right]^H, \\ \mathbf{a}(\theta_{l_{\text{AOD}}}) &= \frac{1}{\sqrt{N_1}} \left[1, e^{-j\frac{2\pi}{\lambda}d\theta_{l_{\text{AOD}}}}, \dots, e^{-j(N-1)\frac{2\pi}{\lambda}d\theta_{l_{\text{AOD}}}} \right]^H. \end{aligned} \quad (3)$$

It is noted that $\theta_{l_{\text{AOA}}} = \sin(\phi_{l_{\text{AOA}}})$ and $\theta_{l_{\text{AOD}}} = \sin(\phi_{l_{\text{AOD}}})$, where $\phi_{l_{\text{AOA}}} \in (-\pi/2, \pi/2)$ and $\phi_{l_{\text{AOD}}} \in (-\pi/2, \pi/2)$ are practical physical angles, and $d = \frac{\lambda}{2}$ is the antenna spacing. $d\theta_{l_{\text{AOA}}}$ ($d\theta_{l_{\text{AOD}}}$) in (3) is the distance difference between the adjacent antennas of the transmitter (receiver) antenna array.

With the discrete Fourier transform (DFT) matrices \mathbf{U}_{f1} and \mathbf{U}_{f2} [19], the above channel model can be presented as $\mathbf{H}_{\text{far-field}}^A$ in angle-domain as follows,

$$\mathbf{H}_{\text{far-field}} = \mathbf{U}_{f2} \mathbf{H}_{\text{far-field}}^A \mathbf{U}_{f1}^H, \quad (4)$$

where $\mathbf{U}_{f1} = [\mathbf{a}(\theta_1), \dots, \mathbf{a}(\theta_{n_1}), \dots, \mathbf{a}(\theta_{N_1})]$ and $\mathbf{U}_{f2} = [\mathbf{a}(\theta_1), \dots, \mathbf{a}(\theta_{n_2}), \dots, \mathbf{a}(\theta_{N_2})]$ are $N_1 \times N_1$ and $N_2 \times N_2$ unitary matrix, where the columns are orthonormal, and $\theta_{n_1} = \frac{2n_1 - N_1 - 1}{N_1}$ with $n_1 = 1, 2, \dots, N_1$, and $\theta_{n_2} = \frac{2n_2 - N_2 - 1}{N_2}$ with $n_2 = 1, 2, \dots, N_2$. Because communication environments have limited scatterers, the angle-domain channel $\mathbf{H}_{\text{far-field}}^A$ often shows sparsity. Some of the existing CS algorithms can utilize this sparsity to solve the channel estimation problem with low pilot overhead [11].

2) *SS-NF Channel Model*: Different from the far-field channel mentioned above, when the distance of the transmitter from the receiver is less than RD, the channel between the transmitter and receiver needs to be modeled under the spherical wave assumption.

Most of the existing near-field channel estimation works consider that only the transmitter employs the extremely large-scale antenna array, while the receivers are usually equipped with a single antenna, i.e., SS-NF scenario. In this case, the antenna of each receiver can be regarded as one element on an antenna array of an equivalent receiver. The near-field channel $\mathbf{H}_{\text{near-field}}$ comprised of the channels between the receivers and the transmitter can be presented as

$$\mathbf{H}_{\text{near-field}} = [\mathbf{h}_{\text{n-f}}^1, \mathbf{h}_{\text{n-f}}^2, \dots, \mathbf{h}_{\text{n-f}}^{N_2}]^H. \quad (5)$$

$\mathbf{h}_{\text{n-f}}^{n_2}$ is the near-field channel between the n_2 -th receiver and the transmitter, which can be represented by

$$\mathbf{h}_{\text{n-f}}^{n_2} = \sqrt{\frac{N_1}{L^{n_2}}} \sum_{l^{n_2}=1}^{L^{n_2}} \alpha_l^{n_2} \mathbf{b}(\theta_l^{n_2}, r_l^{n_2}). \quad (6)$$

For expression simplicity, we assume that $\theta_l = \theta_l^{n_2}$ and $r_l = r_l^{n_2}$ in (6), i.e., $\mathbf{b}(\theta_l, r_l) = \mathbf{b}(\theta_l^{n_2}, r_l^{n_2})$. Different from the far-field channel model in (2), the near-field array response vector $\mathbf{b}(\theta_l, r_l)$ in (6) is derived on the base of spherical wave assumption instead of planar wave assumption, which can presented as [14]

$$\mathbf{b}(\theta_l, r_l) = \frac{1}{\sqrt{N_1}} [e^{-j\frac{2\pi}{\lambda}(r_l^{(1)} - r_l)}, \dots, e^{-j\frac{2\pi}{\lambda}(r_l^{(N_1)} - r_l)}]^H, \quad (7)$$

where r_l denotes the distance of the l -th scatterer from the center of the transmitter antenna array, $r_l^{(n_1)} = \sqrt{r_l^2 + \delta_{n_1}^2 d^2 - 2r_l \delta_{n_1} d \theta_l}$ represents the distance of the l -th scatterer from the n_1 -th transmitter antenna, $\delta_{n_1} = \frac{2n_1 - N_1 - 1}{2}$ with $n_1 = 1, 2, \dots, N_1$, $\theta_l = \sin(\phi_l)$, and $\phi_l \in (-\pi/2, \pi/2)$ are the practical physical angles. By utilizing the Taylor expansion $\sqrt{(1+x)} \approx 1 + \frac{1}{2}x - \frac{1}{8}x^2 + \mathcal{O}(x^2)$, the distance difference $r_l^{(n_1)} - r_l$ in (7) can be approximated by:

$$r_l^{(n_1)} - r_l \approx -\delta_{n_1} d\theta_l + \delta_{n_1}^2 d^2 \frac{(1 - \theta_l^2)}{2r_l}. \quad (8)$$

For the aim to explore the sparsity of the near-field channel, authors in [14] proposed a new transform matrix \mathbf{W} to change the channel $\mathbf{H}_{\text{near-field}}$ in (5) into polar-domain, which can be presented as

$$\mathbf{W} = [\mathbf{b}(\theta_1, r_1^1), \dots, \mathbf{b}(\theta_1, r_1^{S_1}), \dots, \mathbf{b}(\theta_{N_1}, r_{N_1}^1), \dots, \mathbf{b}(\theta_{N_1}, r_{N_1}^{S_{N_1}})], \quad (9)$$

where each column of polar-domain transform matrix \mathbf{W} is a near-field array response vector with the sampled angle θ_{n_1} and distance $r_{n_1}^{s_{n_1}}$, with $s_{n_1} = 1, 2, \dots, S_{n_1}$, S_{n_1} denotes the number of sampled distances at the sampled angle θ_{n_1} . Therefore, we can calculate the number of total sampled grids of the whole propagation environment as $S = \sum_{n_1=1}^{N_1} S_{n_1}$. On the base of this polar-domain transform matrix \mathbf{W} , the near-field channel $\mathbf{h}_{\text{n-f}}^{n_2}$ in (6) can be presented as

$$\mathbf{h}_{\text{n-f}}^{n_2} = \mathbf{W}\mathbf{h}_{\text{n-f}}^{n_2 P}, \quad (10)$$

where $\mathbf{h}_{\text{n-f}}^{n_2 P}$ is the polar-domain channel of size $S \times 1$. As we mentioned before, the far-field channel $\mathbf{H}_{\text{far-field}}$ in (2) shows sparsity in the angle-domain, similarly, this near-field $\mathbf{h}_{\text{n-f}}^{n_2 P}$ in (10) also shows certain sparsity in the polar-domain. The authors in [14] proposed the associated polar-domain based CS algorithm to solve the near-field channel estimation problem.

In the current SS-NF channel model above, the receiver is in the transmitter's near-field region, while the transmitter is in the receivers' far-field region. However, in a certain scenario, the transmitter and receiver can both employ an extremely large-scale antenna array [17] in practice, where the transmitter and the receiver are both in the near-field regions, i.e., *double-side near-field (DS-NF)* scenario. The channel between the transmitter and the receiver in this scenario cannot be modeled by the existing SS-NF channel model accurately. Thus, the existing SS-NF channel estimation algorithms can not be directly utilized to solve the XL-MIMO channel estimation problem accurately. In order to design the channel estimation algorithm for the DS-NF scenario, we should first define the range of the DS-NF region and model the DS-NF channel. The range of DS-NF region and specific DS-NF channel model proposed in our paper will be described Section III and Section IV, respectively.

III. THE DEFINITION OF RAYLEIGH DISTANCE FOR DOUBLE-SIDE NEAR-FIELD SCENARIO

In this section, we will define the double-side near-field Rayleigh distance (DS-RD) and effective double-side near-field Rayleigh distance (EDS-RD) to determine the range of the DS-NF region.

As described in [15], the RD for a SS-NF scenario is defined as $Z = 2D^2/\lambda$, which is calculated by the condition that the maximum allowable phase error between the far-field channel and the near-field channel in the free space is no more than $\pi/8$. However, the current RD is identified based on the SS-NF scenario, where only the transmitter employs the extremely large-scale antenna array while the receiver is equipped with a single antenna. In this paper, by considering the DS-NF scenario, double-side near-field Rayleigh distance (DS-RD) is defined by the condition that the maximum allowable phase error between the DS-NF channel and the far-field channel is no more than $\pi/8$. Then, effective double-side near-field Rayleigh distance (EDS-RD) is defined by the condition that the maximum allowable phase error between the DS-NF channel and the SS-NF channel in the free space is no more than $\pi/8$. The DS-RD and EDS-RD are derived as below.

As shown in Fig. 1, we consider the scenario where the transmitter and receiver are both equipped with extremely large-scale antenna arrays of aperture D_1 and D_2 , respectively, and these two antenna arrays are set in parallel. The center of extremely large-scale antenna arrays of transmitter is regarded as the x-y coordinate origin. The coordinate of the n_1 -th antenna of the transmitter antenna array, the center of receiver antenna array, the n_2 -th antenna of the receiver antenna array are $(0, d_1)$, (x_2, y_2) , and $(x_2, y_2 + d_2)$, respectively, where $-\frac{D_1}{2} \leq d_1 \leq \frac{D_1}{2}$ and $-\frac{D_2}{2} \leq d_2 \leq \frac{D_2}{2}$.

To derive the close form of DS-RD and EDS-RD, we only consider the phase change caused by LoS path component of the channel for expression simplicity. $\mathbf{H}(n_2, n_1)$ represents the LoS path component of channel between the transmitter's n_1 -th antenna and the receiver's n_2 -th antenna, which can be represented as

$$\mathbf{H}(n_2, n_1) = e^{-j2\pi(r_{n_2, n_1} - r)/\lambda}, \quad (11)$$

where r_{n_2, n_1} is the distance of the transmitter's n_1 -th antenna from the receiver's n_2 -th antenna, and r is the distance of the center of transmitter antenna array from the center of receiver antenna array. r_{n_2, n_1} can be presented as

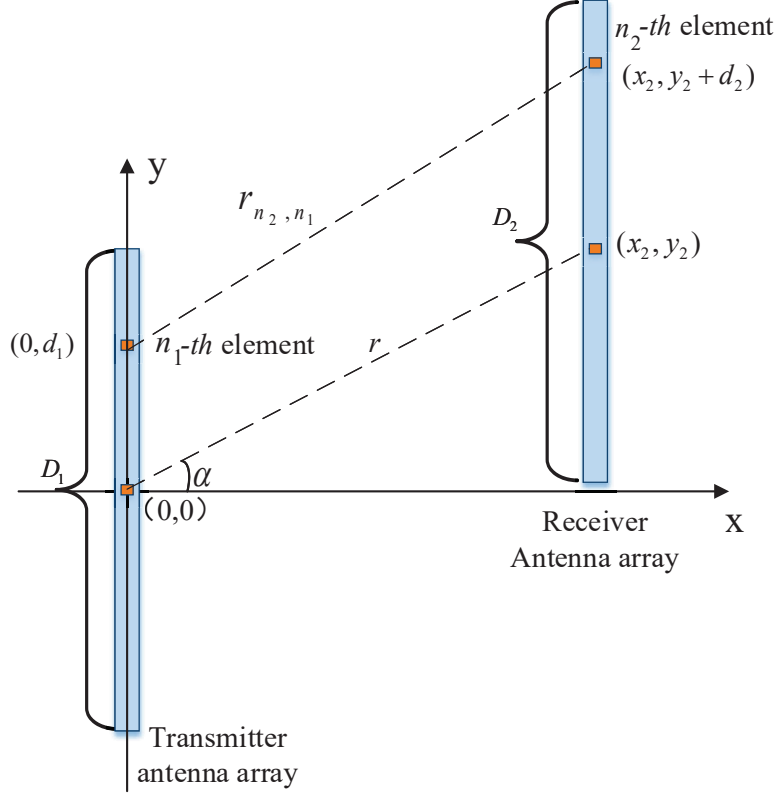


Fig. 1. The double-side near-field scenario: transmitter and receiver are both equipped with extremely large-scale antenna arrays with antenna array elements (orange squares) in the x - y coordinate system

$$r_{n_2, n_1} = \sqrt{(r\alpha + d_2 - d_1)^2 + r^2(1 - \alpha^2)}, \quad (12)$$

where $\alpha = \sin(\phi)$, and ϕ is the practical physical angle. (12) can be further represented as

$$\begin{aligned} r_{n_2, n_1} &= \sqrt{(r\alpha + d_2 - d_1)^2 + r^2(1 - \alpha^2)} \\ &= \sqrt{r^2\alpha^2 + d_2^2 + d_1^2 + 2rad_2 - 2rad_1 - 2d_1d_2 + r^2(1 - \alpha^2)} \\ &= \sqrt{r^2 + (d_2 - d_1)^2 + 2rad_2 - 2rad_1} \\ &= r\sqrt{1 + \frac{(d_2 - d_1)^2}{r^2} + \frac{2\alpha(d_2 - d_1)}{r}}. \end{aligned} \quad (13)$$

By utilizing the Taylor expansion $\sqrt{(1+x)} \approx 1 + \frac{1}{2}x - \frac{1}{8}x^2 + \mathcal{O}(x^2)$, we have

$$\begin{aligned}
r_{n_2, n_1} - r &\approx r \left(1 + \frac{(d_2 - d_1)^2}{2r^2} + \frac{\alpha(d_2 - d_1)}{r} - \frac{1}{8} \left(\frac{2\alpha(d_2 - d_1)}{r} \right)^2 \right) - r \\
&= r \left(1 + \frac{\alpha(d_2 - d_1)}{r} + \frac{(1 - \alpha^2)(d_2 - d_1)^2}{2r^2} \right) - r \\
&= -\alpha d_1 + \frac{(1 - \alpha^2)d_1^2}{2r} + \alpha d_2 + \frac{(1 - \alpha^2)d_2^2}{2r} + \frac{(1 - \alpha^2)d_1 d_2}{r}.
\end{aligned} \tag{14}$$

A. Double-Side Near-Field Rayleigh Distance (DS-RD)

We can observe that the first and third terms in (14), i.e., $-\alpha d_1$ and αd_2 is equal to distance difference of far-field array response vector at transmitter side and receiver side according to (3) in far-field scenario. Thus, the rest terms in (14) determines the maximum allowable phase error between the double DS-NF channel and the far-field channel, i.e., $\frac{(1-\alpha^2)d_1^2}{2r} + \frac{(1-\alpha^2)d_2^2}{2r} + \frac{(1-\alpha^2)d_1 d_2}{r}$ in (14), which can be written as

$$\max \left| \frac{2\pi(1 - \alpha^2)(d_1 + d_2)^2}{r\lambda} \right| \geq \pi/8. \tag{15}$$

It can be easily observed from (15) that when $\alpha = 0$, $d_1 = \frac{D_1}{2}(-\frac{D_1}{2})$ and $d_2 = \frac{D_2}{2}(-\frac{D_2}{2})$, the allowable phase error achieves maximum. Then, we can obtain that

$$r \leq \frac{2(D_1 + D_2)^2}{\lambda}. \tag{16}$$

Thus, the DS-RD can be defined as

$$\text{DS-RD} = \frac{2(D_1 + D_2)^2}{\lambda}. \tag{17}$$

B. Effective Double-Side Near-Field Rayleigh Distance (EDS-RD)

We can observe that the first and second terms in (14), i.e., $-\alpha d_1 + \frac{(1-\alpha^2)d_1^2}{2r}$ is equal to distance difference of near-field array response vector at transmitter side according to (8) in SS-NF scenario. Similarly, the third and fourth term of in (14), i.e., $\alpha d_2 + \frac{(1-\alpha^2)d_2^2}{2r}$ is equal to near-field distance difference of array response vector at receiver side in SS-NF scenario. Thus, the fifth term in (14) determines the maximum allowable phase error between the DS-NF channel and the single near-field channel in the free space, i.e., $\frac{(1-\alpha^2)d_1 d_2}{r}$, which can be written as

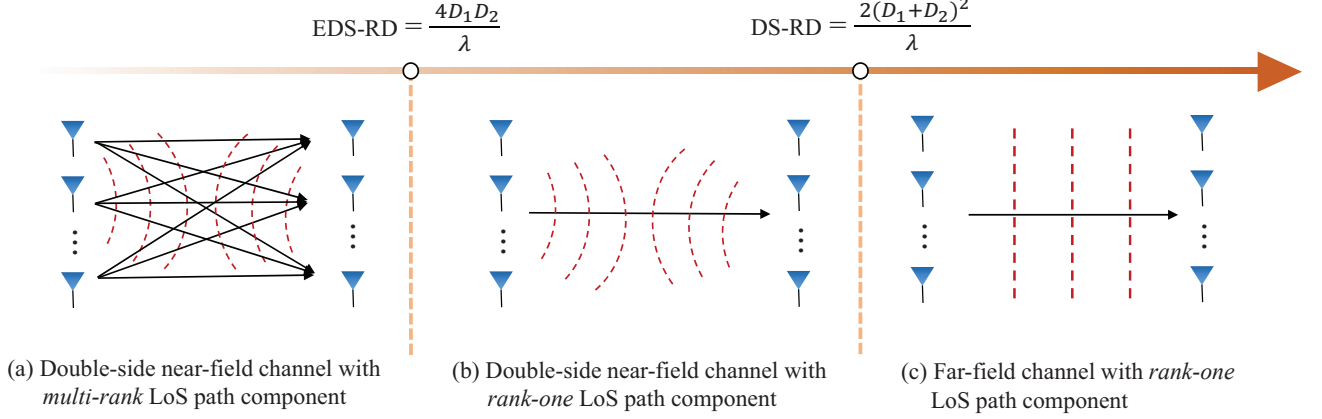


Fig. 2. Three categories of XL-MIMO LoS path component are divided by the distance of the transmitter from the receiver.

$$\max \left| \frac{2\pi(1 - \alpha^2)d_1d_2}{r\lambda} \right| \geq \pi/8. \quad (18)$$

It can be observed from (18) that when $\alpha = 0$, $d_1 = \frac{D_1}{2}$ (or $-\frac{D_1}{2}$) and $d_2 = \frac{D_2}{2}$ (or $-\frac{D_2}{2}$), the allowable phase error is maximal. Then, we can obtain that

$$r \leq \frac{4D_1D_2}{\lambda}. \quad (19)$$

Thus, the EDS-RD can be defined as

$$\text{EDS-RD} = \frac{4D_1D_2}{\lambda}. \quad (20)$$

From the derivation above, the XL-MIMO can be divided into three categories as shown in Fig. 2, where the LoS path component of the XL-MIMO channel has different features with different distances of the transmitter from the receiver. Specifically, when the distance is bigger than the DS-RD, the phase error between the LoS path components of the DS-NF channel and far-field channel can be ignored. Additionally, we can know that when the distance of the transmitter from the receiver is bigger than the EDS-RD and smaller than DS-RD, the phase error between the LoS path components of the DS-NF channel and SS-NF channel can be ignored. In this case, the LoS path component of the DS-NF channel can be modeled by the multiplication of near-field response vectors at transmitter and receiver as that in far-field (2). Thus, the rank of DS-NF LoS path component is only one. Furthermore, when the distance of the transmitter from the receiver is smaller than the EDS-RD, the phase error between the LoS path components of

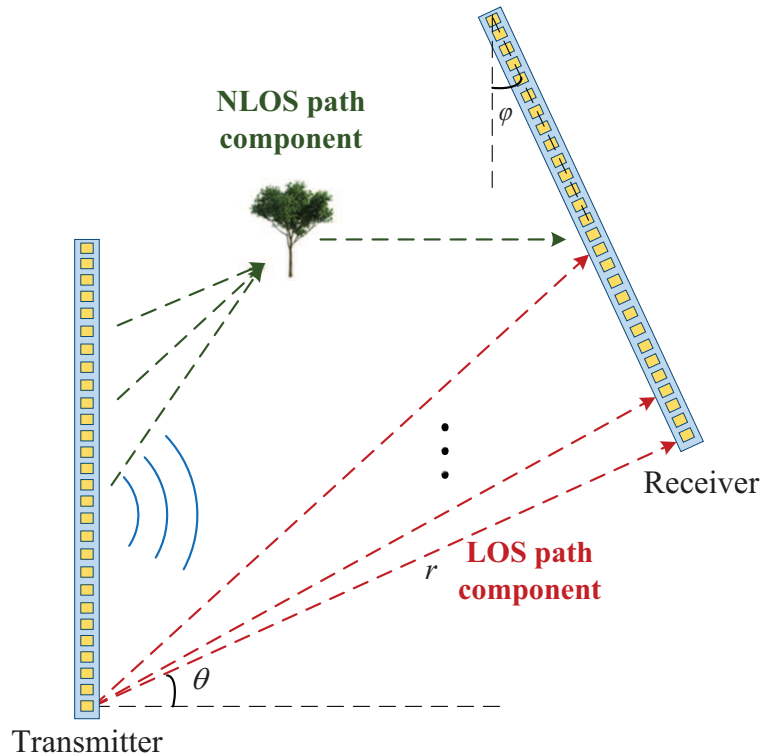


Fig. 3. The proposed double-side near-field channel model for XL-MIMO.

the DS-NF channel and SS-NF channel cannot be ignored. Thus, the rank of the near-field LoS path component may be very large.

In this paper, we consider the scenario that the distance of the transmitter from the receiver is smaller than the EDS-RD. In the following Section IV, the specific DS-NF channel model will be described.

IV. PROPOSED DS-NF CHANNEL MODEL FOR XL-MIMO

In this section, we propose a DS-NF channel model under the condition that the distance of the transmitter from receiver is smaller than the EDS-RD. Two different kinds of path components for the DS-NF channel are shown in Fig. 3. The NLoS path and LoS path components in Fig. 3 should be modeled separately.

A. NLoS Path Component

For NLoS path components, where the transmitter signal focuses on the scatterers first and then transmit to the receiver as shown in Fig. 3, the near-field array response vector is utilized to replace the far-field array response vector in (2), which is presented as

$$\mathbf{H}_{\text{NLoS}} = \sum_{l=1}^L g_l \mathbf{b}(\theta_r^l, d_r^l) \mathbf{b}^H(\theta_t^l, d_t^l) \quad (21)$$

where L denotes the number of NLoS path components, g_l represents the complex gain. $\mathbf{b}(\theta_t^l, d_t^l)$ and $\mathbf{b}(\theta_r^l, d_r^l)$ denote the near-field array response vector at transmitter and receiver on the base of spherical wave assumption, which is denoted by

$$\begin{aligned} \mathbf{b}(\theta_t^l, d_t^l) &= \frac{1}{\sqrt{N_1}} [e^{-j\frac{2\pi}{\lambda}(d_t^l(1)-d_t^l)}, \dots, e^{-j\frac{2\pi}{\lambda}(d_t^l(N_1)-d_t^l)}]^H, \\ \mathbf{b}(\theta_r^l, d_r^l) &= \frac{1}{\sqrt{N_2}} [e^{-j\frac{2\pi}{\lambda}(d_r^l(1)-d_r^l)}, \dots, e^{-j\frac{2\pi}{\lambda}(d_r^l(N_2)-d_r^l)}]^H, \end{aligned} \quad (22)$$

where θ_t^l (θ_r^l) represent the angle for the l -th path at transmitter (receiver), and d_t^l (d_r^l) represent the distance of the l -th scatterer from the center of the antenna array of transmitter (receiver) for the l -th path, $d_t^l(n_1) = \sqrt{d_t^l{}^2 + \delta_{n_1}^2 d^2 - 2d_t^l \delta_{n_1} d \theta_t^l}$ represents the distance of the l -th scatterer from the n_1 -th element on transmitter antenna array, and $\delta_{n_1} = \frac{2n_1 - N_1 - 1}{2}$ with $n = 1, 2, \dots, N_1$, and $d_r^l(n_2) = \sqrt{d_r^l{}^2 + \delta_{n_2}^2 d^2 - 2d_r^l \delta_{n_2} d \theta_r^l}$ represents the distance of the l -th scatterer from the n_2 -th transmitter antenna array, and $\delta_{n_2} = \frac{2n_2 - N_2 - 1}{2}$ with $n = 1, 2, \dots, N_2$.

The polar-domain transform matrix mentioned in (9) can be presented as

$$\begin{aligned} \mathbf{W}_t &= [\mathbf{b}(\theta_1, d_1^1), \dots, \mathbf{b}(\theta_1, d_1^{S_1}), \dots, \\ &\quad \mathbf{b}(\theta_{N_1}, d_{N_1}^1), \dots, \mathbf{b}(\theta_{N_1}, d_{N_1}^{S_{N_1}})], \\ \mathbf{W}_r &= [\mathbf{b}(\theta_1, r_1^1), \dots, \mathbf{b}(\theta_1, r_1^{S_1}), \dots, \\ &\quad \mathbf{b}(\theta_{N_2}, r_{N_2}^1), \dots, \mathbf{b}(\theta_{N_2}, r_{N_2}^{S_{N_2}})], \end{aligned} \quad (23)$$

where each column of the matrix \mathbf{W}_t (\mathbf{W}_r) is near-field array response vector with the specific sampled angle θ_{n_1} (θ_{n_2}) and sampled distance $d_{n_1}^{s_{n_1}}$ ($d_{n_2}^{s_{n_2}}$), with $s_n = 1, 2, \dots, S_{n_1}$ (S_{n_2}). S_{n_1} (S_{n_2}) denotes the number of sampled distances at the sampled angle θ_{n_1} (θ_{n_2}). Therefore, we can calculate the total number of all sampled grids, i.e., the number of \mathbf{W}_t (\mathbf{W}_r) columns, which can be presented as $S_1 = \sum_{n_1=1}^N S_{n_1}$ ($S_2 = \sum_{n_2=1}^N S_{n_2}$).

On the base of this polar-domain transform matrix \mathbf{W}_t and \mathbf{W}_r , the channel \mathbf{H}_{NLoS} can be represented by

$$\mathbf{H}_{\text{NLoS}} = \mathbf{W}_r \mathbf{H}_{\text{NLoS}}^P \mathbf{W}_t^H, \quad (24)$$

where $\mathbf{H}_{\text{NLoS}}^P$ is the $S_2 \times S_1$ polar-domain channel.

B. LoS Path Component

As mentioned in Section III-B, there is still phase error between the DS-NF channel and SS-NF channel when the distance of the transmitter from the receiver is smaller than EDS-RD. Thus, in this case, the channel model built with the near-field array response vector will mismatch the practical feature of DS-NF LoS path component. As a result, instead of utilizing near-field array response vector like NLoS path components, we model the LoS path component under the geometric free space assumption [20], which can be represented as

$$\mathbf{H}_{\text{LoS}} = \left[\frac{1}{r_{n_2, n_1}} e^{-j2\pi r_{n_2, n_1} / \lambda} \right]_{N_2 \times N_1}, \quad (25)$$

where r_{n_2, n_1} denotes the distance of the n_1 -th antenna at receiver from the n_2 -th antenna at transmitter. The r_{n_2, n_1} can be represented as

$$r_{n_2, n_1} = \sqrt{r^2 + d_1^2 + d_2^2 + 2rd_2 \sin(\varphi - \theta) - 2rd_1 \sin(\theta) - 2d_1d_2 \cos(\varphi)} \quad (26)$$

where the r is the distance of the 1-st antenna at receiver from the 1-st antenna at transmitter, φ denotes relative angle between receiver and transmitter, and θ denotes the AoA of the signal. Unlike the NLoS path components, the LoS path component cannot be decoupled by a near-field array response vector. Thus, the LoS path component can not be presented by polar-domain channel with transform matrices.

It is worth noting that the LoS path component will degenerate into the same representation as NLoS path components of DS-NF channel model when the distance of the transmitter from the receiver is greater than the EDS-RD.

C. Proposed DS-NF Channel

According to the NLoS path components and LoS path component mentioned above, the DS-NF channel can be presented as

$$\begin{aligned}
\mathbf{H}_{\text{DS-NF}} &= \mathbf{H}_{\text{LoS}} + \mathbf{H}_{\text{NLoS}} \\
&= \left[\frac{1}{r_{n_2, n_1}} e^{-j2\pi r_{n_2, n_1}/\lambda} \right]_{N_2 \times N_1} + \mathbf{W}_r \mathbf{H}_{\text{NLoS}}^P \mathbf{W}_t^H.
\end{aligned} \tag{27}$$

In the next Section V, based on the proposed DS-NF channel model, a channel estimation scheme will be proposed to estimate LoS path component and NLoS path components separately.

V. PROPOSED DS-NF CHANNEL ESTIMATION ALGORITHM

In this section, based on the proposed DS-NF channel model, we propose the corresponding DS-NF channel estimation algorithm, where a hierarchical parameter estimation algorithm is utilized for the LoS path component estimation and an OMP-based algorithm is utilized for the NLoS path components estimation. At last, we analyze the computational complexity of the proposed DS-NF algorithm.

A. LoS Path Component Estimation: Hierarchical Parameter Estimation

Since the energy of LoS path component is dominant, we will first conduct the LoS path component estimation. From (25), we can observe that the LoS path component of DS-NF channel is determined by three parameters, i.e., the distance of the 1-st antenna at receiver from the 1-st antenna at transmitter r , relative angle between receiver and transmitter φ , and the AoA of the signal θ . Therefore, the channel estimation of LoS path component can be recognized as a parameter estimation problem, which can be presented as

$$\begin{aligned}
&\min_{r, \theta, \varphi} \left\| \mathbf{Y} - \left[\frac{1}{r_{n_2, n_1}} e^{-j2\pi r_{n_2, n_1}/\lambda} \right]_{N_2 \times N_1} \mathbf{P} \right\|_F^2, \\
&\text{s.t. } (r, \theta, \varphi) \in \Xi.
\end{aligned} \tag{28}$$

Ξ can be denoted as

$$\begin{aligned}
\Xi &= \{(r, \theta, \varphi) \mid \\
&\quad r = r_{\min}, r_{\min} + \Delta r, \dots, r_{\max}; \\
&\quad \theta = \theta_{\min}, \theta_{\min} + \Delta\theta, \dots, \theta_{\max}; \\
&\quad \varphi = \varphi_{\min}, \varphi_{\min} + \Delta\varphi, \dots, \varphi_{\max}\},
\end{aligned} \tag{29}$$

where r_{\min} , r_{\max} , θ_{\min} , θ_{\max} , φ_{\min} , and φ_{\max} represent the lower and upper boundaries of the distance of the 1-st antenna at receiver antenna array from the 1-st antenna at transmitter antenna array r , relative angle between receiver and transmitter φ , and the AoA of the signal θ , respectively. Δr , $\Delta\theta$, and $\Delta\varphi$ are the step sizes of r , θ , and φ .

It is obvious that the exhaustive search can be utilized to solve problem (28), obtaining the optimal parameters r^{opt} , θ^{opt} , φ^{opt} from the grid collection Ξ . However, the exhaustive search over a dense grid collection is time-consuming. To reduce the overhead of searching, we can increase the step sizes Δr , $\Delta\theta$, and $\Delta\varphi$ to reduce the number of the grids in Ξ . But the performance of the channel estimation will also degrade accordingly, since the grid is too coarse. In order to solve this problem, we design hierarchical grids collections.

Specifically, we assume there are M levels of different grids collections. Moreover, we define a step control factor δ , which is the number of grids in each level of grids collection. In m -th grids collection ($m = 1, 2, \dots, M$), the corresponding Ξ can be defined as

$$\begin{aligned} \Xi^m = \{ & (r^m, \theta^m, \varphi^m) \mid \\ & r^m = r_{\min}^m, r_{\min}^m + \Delta r^m, \dots, r_{\max}^m; \\ & \theta^m = \theta_{\min}^m, \theta_{\min}^m + \Delta\theta^m, \dots, \theta_{\max}^m; \\ & \varphi^m = \varphi_{\min}^m, \varphi_{\min}^m + \Delta\varphi^m, \dots, \varphi_{\max}^m \}. \end{aligned} \quad (30)$$

Let $(r^{m_{\text{opt}}}, \theta^{m_{\text{opt}}}, \varphi^{m_{\text{opt}}})$ denote the optimal grid in Ξ^m for problem (28). Based on $(r^{m_{\text{opt}}}, \theta^{m_{\text{opt}}}, \varphi^{m_{\text{opt}}})$ and $(\Delta r^m, \Delta\theta^m, \Delta\varphi^m)$ of m -th level of grids collection, the $(m+1)$ -th level of grids collection Ξ^{m+1} can be generated, where boundaries and step sizes of (r, θ, φ) can be presented as

$$\begin{aligned} r_{\min}^{m+1} &= r_{\min}^m - \Delta r^m, r_{\max}^{m+1} = r_{\max}^m + \Delta r^m, \Delta r^{m+1} = \Delta r^m / \delta; \\ \theta_{\min}^{m+1} &= \theta_{\min}^m - \Delta\theta^m, \theta_{\max}^{m+1} = \theta_{\max}^m + \Delta\theta^m, \Delta\theta^{m+1} = \Delta\theta^m / \delta; \\ \varphi_{\min}^{m+1} &= \varphi_{\min}^m - \Delta\varphi^m, \varphi_{\max}^{m+1} = \varphi_{\max}^m + \Delta\varphi^m, \Delta\varphi^{m+1} = \Delta\varphi^m / \delta. \end{aligned} \quad (31)$$

Based on the hierarchical grids collection, the basic idea of LoS path component estimation is to search from the 1-st level grids collection to the M -th level grids collection in turn, where the boundaries and step sizes of the latter level of grids collection are updated by the optimal grid searched by the former level grids collection and step control factor δ based on (31).

Algorithm 1 shows the specific LoS path component estimation procedure, where the searching of optimal grid is divided into M stages. In m -th stage, Steps 2-5 are performed to search the optimal grid $r^{m_{\text{opt}}}, \theta^{m_{\text{opt}}}, \varphi^{m_{\text{opt}}}$ in m -th grids collections. Then, based on $r^{m_{\text{opt}}}, \theta^{m_{\text{opt}}}, \varphi^{m_{\text{opt}}}$,

Algorithm 1 LoS path component estimation

Inputs: \mathbf{Y} , \mathbf{P} , R_{max} , R_{min} , θ_{max} , θ_{min} , φ_{max} , φ_{min} , M , δ , r_s , θ_s , φ_s .

Initialization: $\Delta r_1 = \frac{r_{max}-r_{min}}{r_s}$, $\Delta\theta_1 = \frac{\theta_{max}-\theta_{min}}{\theta_s}$, $\Delta\varphi_1 = \frac{\varphi_{max}-\varphi_{min}}{\varphi_s}$,

calculate Ξ^1 based on (29)

1. **for** $m = 1, 2, \dots, M$ **do**
2. **for** $(r, \theta, \varphi) \in \Xi^m$ **do**
3. calculate \mathbf{H}_{LoS}^* based on (25)
4. $r^{m,opt}, \theta^{m,opt}, \varphi^{m,opt} = \underset{r, \theta, \varphi}{\operatorname{argmin}} \|\mathbf{Y} - \mathbf{H}_{LoS}^m \mathbf{P}\|_2^2$
5. **end for**
6. calculate bounds and step sizes based on (31)
7. generate Ξ^{m+1} based on (30)
8. **end for**
9. $(r^{opt}, \theta^{opt}, \varphi^{opt}) = (r^{M,opt}, \theta^{M,opt}, \varphi^{M,opt})$
10. calculate $\hat{\mathbf{H}}_{LoS}$ based on (25) by $(r^{opt}, \theta^{opt}, \varphi^{opt})$

Output: Estimated LoS path component $\hat{\mathbf{H}}_{LoS}$.

Ξ^{m+1} is calculated by Steps 6-7. Next, the optimal grid $(r^{M,opt}, \theta^{M,opt}, \varphi^{M,opt})$ for the M -th level grids collection is regarded as the searched globally optimal grid $(r^{opt}, \theta^{opt}, \varphi^{opt})$ in the hierarchical grid collections. Finally, $(r^{opt}, \theta^{opt}, \varphi^{opt})$ can be utilized to calculate estimated LoS path component $\hat{\mathbf{H}}_{LoS}$ based on (25).

After obtaining the $\hat{\mathbf{H}}_{LoS}$, we can eliminate the influence of $\hat{\mathbf{H}}_{LoS}$ on the received pilots \mathbf{Y} and then estimate the $\hat{\mathbf{H}}_{NLoS}$.

B. NLoS Path Components Estimation: OMP-Based Estimation

As we already acquire $\hat{\mathbf{H}}_{LoS}$, the received pilots without the effect of $\hat{\mathbf{H}}_{LoS}$ can be presented as

$$\mathbf{Y}_{NLoS} = \mathbf{Y} - \hat{\mathbf{H}}_{LoS} \mathbf{P}. \quad (32)$$

On the base of the polar-domain representation (24), the \mathbf{Y}_{NLoS} can be presented as

$$\mathbf{Y}_{NLoS} = \mathbf{H}_{NLoS} \mathbf{P} + \mathbf{N} = \mathbf{W}_r \mathbf{H}_{NLoS}^P \mathbf{W}_t^H \mathbf{P} + \mathbf{N}. \quad (33)$$

Utilizing $\operatorname{vec}(\mathbf{ABC}) = (\mathbf{C}^T \otimes \mathbf{A}) \operatorname{vec}(\mathbf{B})$ [21], we can reformulate (33) as

$$\mathbf{y}_{NLoS} = ((\mathbf{P}^T \mathbf{W}_t) \otimes \mathbf{W}_r) \mathbf{h}_{NLoS}^P + \mathbf{n} = \mathbf{A} \mathbf{h}_{NLoS}^P + \mathbf{n} \quad (34)$$

where $\mathbf{y}_{\text{NLoS}} = \text{vec}(\mathbf{Y}_{\text{NLoS}})$, $\mathbf{h}_{\text{NLoS}}^P = \text{vec}(\mathbf{H}_{\text{NLoS}}^P)$, $\mathbf{n} = \text{vec}(\mathbf{N})$. As mentioned above, $\mathbf{h}_{\text{NLoS}}^P$ is sparse in polar-domain, thus the NLoS path components estimation is reformulated as a sparse recovery problem. In this sparse recovery problem, the NLoS path components sensing matrix can be denoted as $\mathbf{A} = (\mathbf{P}^T \mathbf{W}_t) \otimes \mathbf{W}_r$. The specific OMP-based algorithm to solve this problem can be summarized in **Algorithm 2**.

Algorithm 2 NLoS path components estimation

Inputs: \mathbf{Y}_{NLoS} , \mathbf{P} , \mathbf{W}_r , \mathbf{W}_t , L .

Initialization: vectorize \mathbf{Y}_{NLoS} as \mathbf{y}_{NLoS} ; $\Omega = \emptyset$, $\mathbf{r} = \mathbf{y}_{\text{NLoS}}$.

1. $\mathbf{A} = (\mathbf{P}^T \mathbf{W}_t) \otimes \mathbf{W}_r$
2. **for** $l = 1, 2, \dots, L$ **do**
3. $n^* = \underset{n=1,2,\dots,S_1 S_2}{\text{argmax}} \|\mathbf{A}^H(:, n) \mathbf{r}\|_2^2$
4. $\Omega = \Omega \cup n^*$
5. $\hat{\mathbf{h}}_A = \mathbf{0}_{N \times 1}$
6. $\hat{\mathbf{h}}_A(\Omega) = \mathbf{A}^\dagger(:, \Omega) \mathbf{y}_{\text{NLoS}}$
7. $\mathbf{r} = \mathbf{y}_{\text{NLoS}} - \mathbf{A} \hat{\mathbf{h}}_A$
8. **end for**
9. reshape $\hat{\mathbf{h}}_A$ into $\hat{\mathbf{H}}_A$ of size $S_2 \times S_1$
10. $\hat{\mathbf{H}}_{\text{NLoS}} = \mathbf{W}_r \hat{\mathbf{H}}_A \mathbf{W}_r^H$

Output: Estimated NLoS path components $\hat{\mathbf{H}}_{\text{NLoS}}$.

Specifically, since there are L components in the polar-domain, we will conduct L iterations to find L supports. In l -th iteration, we will calculate the correlation between the sensing matrix \mathbf{A} and the residual vector \mathbf{r} . In Step 4, we obtain the updated support Ω . Then, in Step 6, the currently estimated near-field NLoS path component $\hat{\mathbf{h}}_A$ is calculated by the least square (LS) algorithm. In Step 9, when L iterations are performed, the $\hat{\mathbf{h}}_A$ need to be reshaped into $\hat{\mathbf{H}}_A$ in the polar-domain of the size $S_2 \times S_1$. Finally, using $\hat{\mathbf{H}}_{\text{NLoS}} = \mathbf{W}_r \hat{\mathbf{H}}_A \mathbf{W}_r^H$, we can obtain the final estimated NLoS path components.

After estimating the near-field LoS path component and the NLoS paths components, the $\hat{\mathbf{H}}_{\text{DS-NF}}$ can be written as

$$\hat{\mathbf{H}}_{\text{DS-NF}} = \hat{\mathbf{H}}_{\text{LoS}} + \hat{\mathbf{H}}_{\text{NLoS}}. \quad (35)$$

C. Computational Complexity Analysis

For the proposed DS-NF channel estimation algorithm, we analyze its computational complexity of as follows. In the stage of the LoS path component estimation, we can observe that the complexity mainly comes from **Algorithm 1** Steps 3-4. In Steps 3-4, we need to compute the $\mathbf{H}_{\text{LoS}}^*$ according to (25) in m -th level of codebook and find the best codeword. Therefore, the complexity of this part is $\mathcal{O}(N_1 N_2 S_{\text{LoS}})$, where S_{LoS} is the size of the codebook. After M iterations, the total complexity of the LoS path component estimation is $\mathcal{O}(M N_1 N_2 S_{\text{LoS}})$. For the NLoS path components estimation, the computational complexity can be obtained as $\mathcal{O}(S_1 S_2 N_1 N_2 L^3)$ by referring to the OMP algorithm [10].

VI. SIMULATION RESULT

In this section, we conduct the simulations to verify the performance of the proposed channel estimation algorithm for the proposed DS-NF channel model in the DS-NF scenario. The system parameters are as follows: the number of antenna of transmitter is $N_1 = 128$, the number of antenna of receiver is $N_2 = 64$. The carrier frequency is $f = 10$ GHz, corresponding to $\lambda = 0.03$ m. By utilizing (20), the EDS-RD can be calculated as $\frac{4D_1 D_2}{\lambda} = \frac{4(N_1 \lambda / 2)(N_2 \lambda / 2)}{\lambda} = 245.76$ m in this scenario. The near-field channel in (21) contains $L = 5$ NLoS path components. Meanwhile, the sampled angles of arrival follow the uniform distribution $\mathcal{U}(-\frac{\pi}{3}, \frac{\pi}{3})$. The distances are generated in range of [20, 260] meters. The pilot matrix \mathbf{P} randomly chooses its elements of the from $\{-\frac{1}{\sqrt{M}}, +\frac{1}{\sqrt{M}}\}$. The total number of the sampled grids of the whole propagation environment for the polar-domain transform matrix \mathbf{W}_t and \mathbf{W}_r is set to $S_1 = 254$ and $S_2 = 64$, which is generated according to the method describe in [14].

We compare the proposed DS-NF channel estimation algorithm and the existing SS-NF OMP method [14] and far-field OMP method [10]. The normalized mean square error (NMSE) performance, which is defined as $\text{NMSE} = \frac{\mathbb{E}(\|\mathbf{H} - \hat{\mathbf{H}}\|_2^2)}{\mathbb{E}(\|\mathbf{H}\|_2^2)}$, is used to evaluate the accuracy of different methods.

Fig. 4 depicts the NMSE performance comparison with respect to the distance of the transmitter from the receiver. The range of distance is from 20 m to 260 m. The SNR is 5dB and the size of pilot matrix is 128×64 , the compressive ratio is $\frac{M}{N_1} = 0.5$. The proposed DS-NF scheme can achieve better NMSE performance than the existing far-field OMP scheme and the SS-NF OMP scheme. Specifically, the NMSE of the proposed algorithm is robust and remains the lowest value of all the schemes in the whole range of distance. The NMSE performance of the existing

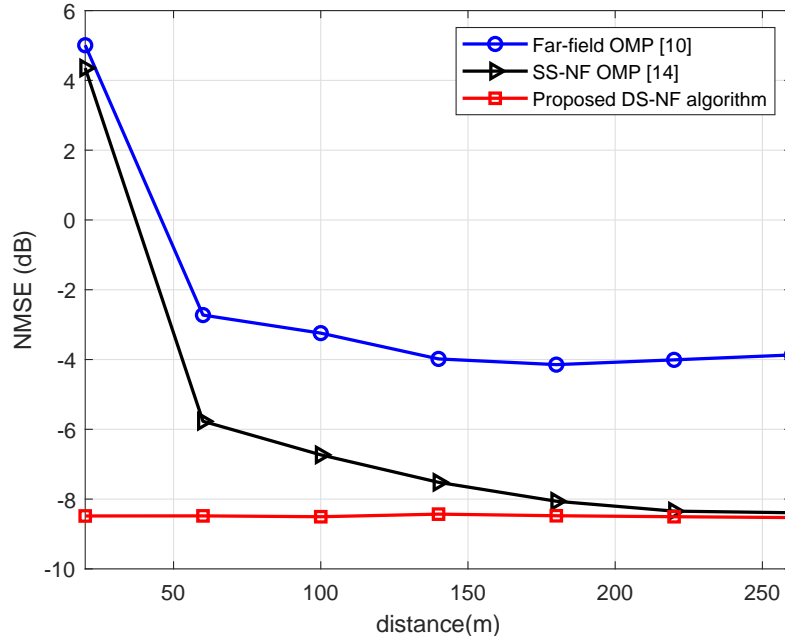
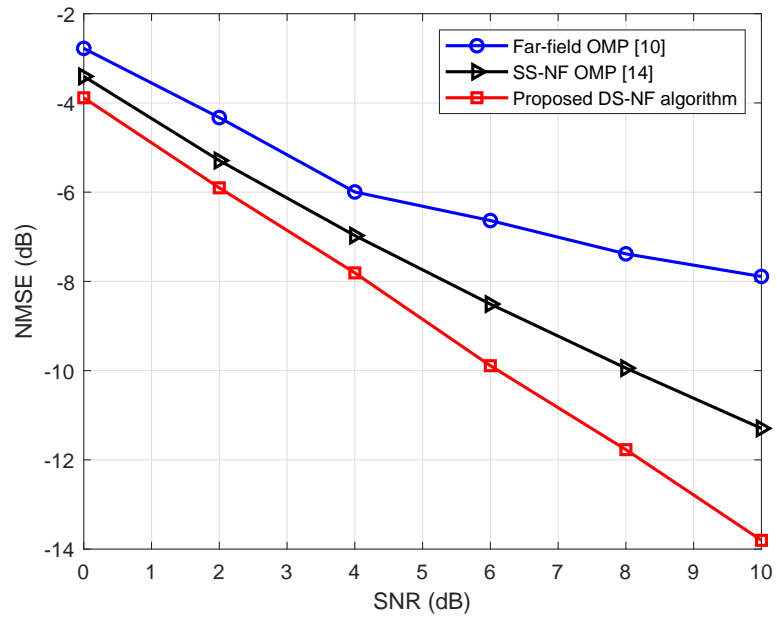


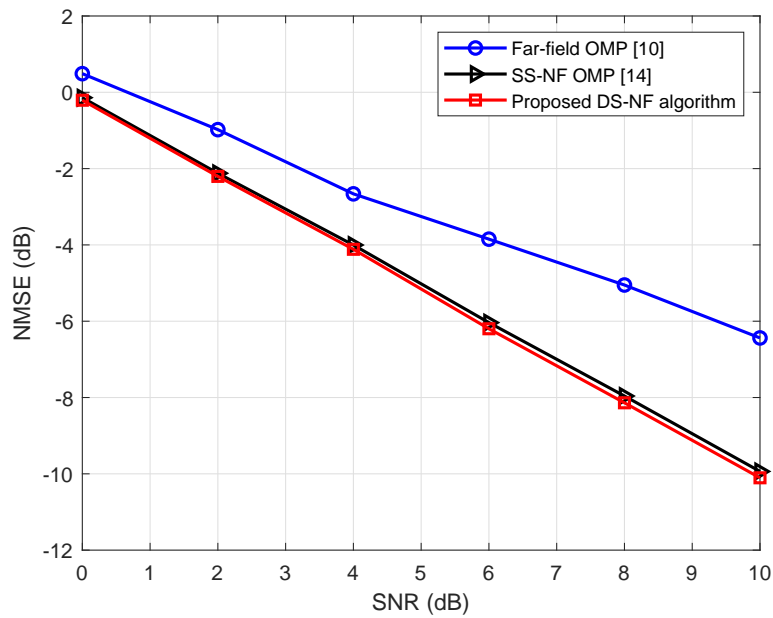
Fig. 4. NMSE performance comparison with respect to the distance of the transmitter from the receiver.

far-field OMP scheme and the SS-NF OMP scheme degrade gradually with the decrease of the distance. The reason is that there are still phase errors between the proposed DS-NF channel and the existing far-field channel as well as the SS-NF channel. In other words, the existing two channel models mismatch the feature of DS-NF scenario. The NMSE of the SS-NF OMP scheme can reach a low NMSE only when the distance is larger than 220 m, which is a little smaller than the EDS-RD 245.76 m. When the distance is large than 220 m, the performance of the proposed scheme and the SS-NF OMP channel estimation show the same performance. This is because when the distance is large than EDS-RD but smaller than DS-RD, the phase error between the DS-NF channel model and the SS-NF model vanishes.

Fig. 5 shows the NMSE performance comparison with respect to the SNR under different distances, where the size of pilot is 128×64 . In Fig. 5 (a) and (b), the distance is 40 m and 150 m, respectively. We can see that when the distance is small, the proposed DS-NF channel estimation scheme outperforms all the other schemes. In particular, when SNR is 6 dB, the proposed scheme can achieve about 2 dB improvement compared with the SS-NF OMP scheme. The reason is that the existing schemes cannot deal with the LoS path component of DS-NF channel model. Furthermore, we can see that, in the Fig. 5 (b), the performance gap of NMSE of the three schemes is small in the range of all the SNRs.

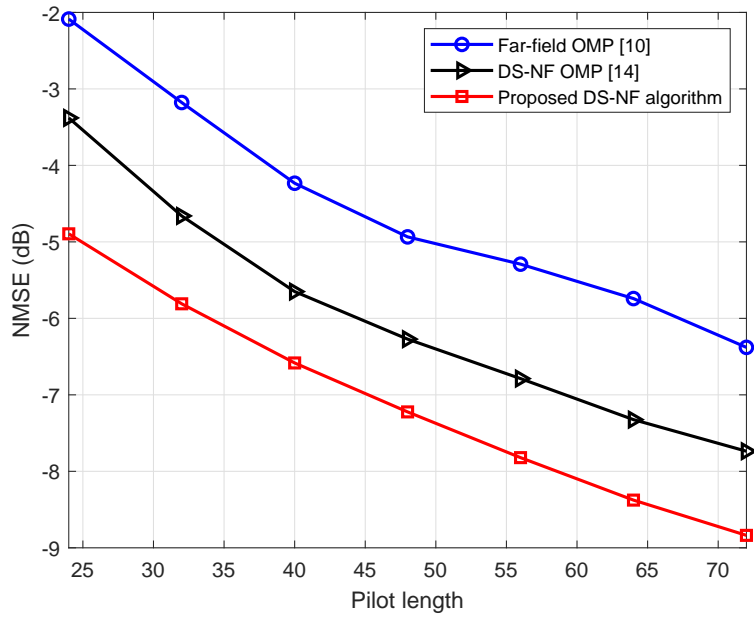


(a)

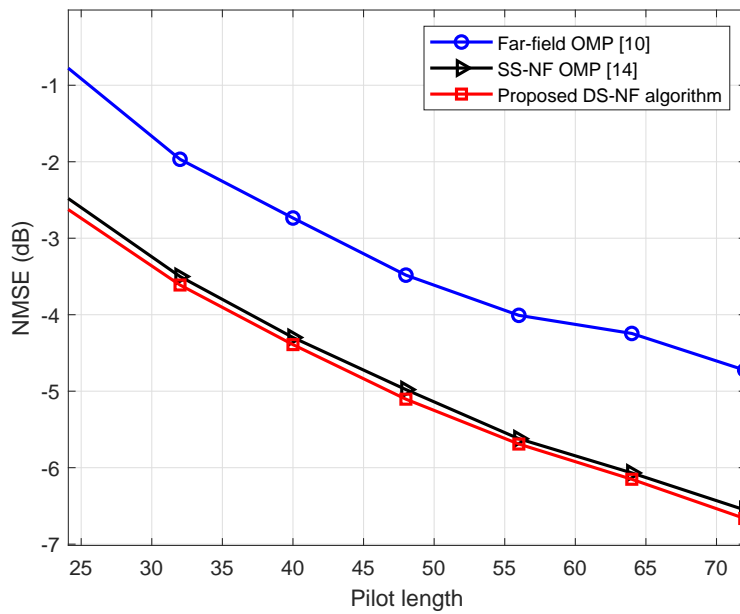


(b)

Fig. 5. NMSE performance comparison with respect to the SNR under different distances. (a) $r = 40$ m; (b) $r = 150$ m.



(a)



(b)

Fig. 6. NMSE performance with respect to the size of the pilot. (a) $r = 40$ m; (b) $r = 150$ m.

Fig. 6 depicts the NMSE performance comparison with respect to the size of the pilot P , where the SNR is 5dB. The proposed scheme achieves the best performance out of all three considered schemes. When the distance becomes large as shown in Fig. 6 (b), the NMSE achieved by the DS-NF channel estimation scheme and other schemes are similar. When the distance is small as shown in Fig. 6 (a), the proposed scheme outperforms all the other schemes.

VII. CONCLUSIONS

In this paper, the channel estimation of DS-NF scenario for XL-MIMO wireless communication system was investigated. We derived the range of the DS-NF region, i.e., effective double-side near-field Rayleigh distance (EDS-RD). Then we proposed the DS-NF channel model, where the distance of the transmitter from receiver is smaller than EDS-RD. In the proposed channel model, the LoS and NLoS path components were characterized by the near-field response vector and geometric free space assumption, respectively. It is worth pointing out that the DS-NF channel model proposed in this paper can be recognized as the generalization of the current far-field channel model as well as the SS-NF channel model for MIMO systems. Simulation results showed that, compared with the far-field and SS-NF channel estimation, the proposed DS-NF channel estimation scheme achieved better NMSE performance. For future work, based on the proposed new DS-NF channel model, the beam training problem will attract further research interest.

REFERENCES

- [1] Z. Zhang, Y. Xiao, Z. Ma, M. Xiao, Z. Ding, X. Lei, G. K. Karagiannidis, and P. Fan, "6G wireless networks: Vision, requirements, architecture, and key technologies," *IEEE Veh. Technol. Mag.*, vol. 14, no. 3, pp. 28–41, Sep. 2019.
- [2] P. P. Ray, N. Kumar, and M. Guizani, "A vision on 6G-enabled NIB: Requirements, technologies, deployments, and prospects," *IEEE Wireless Commun.*, vol. 28, no. 4, pp. 120–127, May 2021.
- [3] M. Giordani, M. Polese, M. Mezzavilla, S. Rangan, and M. Zorzi, "Toward 6G networks: Use cases and technologies," *IEEE Commun. Mag.*, vol. 58, no. 3, pp. 55–61, Mar. 2020.
- [4] E. D. Carvalho, A. Ali, A. Amiri, M. Angelichinoski, and R. W. Heath, "Non-stationarities in extra-large-scale massive MIMO," *IEEE Wireless Commun.*, vol. 27, no. 4, pp. 74–80, Aug. 2020.
- [5] V. Croisfelt, A. Amiri, T. Abrao, E. de Carvalho, and P. Popovski, "Accelerated randomized methods for receiver design in extra-large scale MIMO arrays," *IEEE Trans. Veh. Technol.*, vol. 70, no. 7, pp. 6788–6799, May 2021.
- [6] X. Ma, Z. Gao, F. Gao, and M. Di Renzo, "Model-driven deep learning based channel estimation and feedback for millimeter-wave massive hybrid mimo systems," *IEEE J. Sel. Areas Commun.*, vol. 39, no. 8, pp. 2388–2406, Jun. 2021.
- [7] X. Li, X. Zhang, Y. Zhou, and L. Hanzo, "Optimal massive-MIMO-aided clustered base-station coordination," *IEEE Trans. Veh. Technol.*, vol. 70, no. 3, pp. 2699–2712, Feb. 2021.

- [8] S. Sun, T. S. Rappaport, R. W. Heath, A. Nix, and S. Rangan, "MIMO for millimeter-wave wireless communications: beamforming, spatial multiplexing, or both?" *IEEE Commun. Mag.*, vol. 52, no. 12, pp. 110–121, Dec. 2014.
- [9] A. Adhikary, J. Nam, J.-Y. Ahn, and G. Caire, "Joint spatial division and multiplexing-The large-scale array regime," *IEEE Trans. Inf. Theory*, vol. 59, no. 10, pp. 6441–6463, Oct. 2013.
- [10] J. Lee, G. Gil, and Y. H. Lee, "Channel estimation via orthogonal matching pursuit for hybrid MIMO systems in millimeter wave communications," *IEEE Trans. Commun.*, vol. 64, no. 6, pp. 2370–2386, Jun. 2016.
- [11] X. Wei and L. Dai, "Channel estimation for extremely large-scale massive MIMO: Far-field, near-field, or hybrid-field?" *IEEE Communications Letters*, vol. 26, no. 1, pp. 177–181, Jan. 2022.
- [12] Y. Jin, J. Zhang, B. Ai, and X. Zhang, "Channel estimation for mmwave massive MIMO with convolutional blind denoising network," *IEEE Commun. Lett.*, vol. 24, no. 1, pp. 95–98, Jan. 2020.
- [13] Y. Han, S. Jin, C. Wen, and X. Ma, "Channel estimation for extremely large-scale massive MIMO systems," *IEEE Wireless Commun. Lett.*, vol. 9, no. 5, pp. 633–637, May 2020.
- [14] M. Cui and L. Dai, "Channel estimation for extremely large-scale MIMO: Far-field or near-field," *IEEE Trans. Commun. (early access)*, Jan. 2022.
- [15] K. T. Selvan and R. Janaswamy, "Fraunhofer and Fresnel distances: Unified derivation for aperture antennas," *IEEE Antennas Propag. Mag.*, vol. 59, no. 4, pp. 12–15, Aug. 2017.
- [16] X. Yin, S. Wang, N. Zhang, and B. Ai, "Scatterer localization using largescale antenna arrays based on a spherical wave-front parametric model," *IEEE Trans. Wireless Commun.*, vol. 16, no. 10, pp. 6543–6556, Jul. 2017.
- [17] D. Dardari, "Communicating with large intelligent surfaces: Fundamental limits and models," *IEEE J. Sel. Areas Commun.*, vol. 38, no. 11, pp. 2526–2537, Nov. 2020.
- [18] Z. Wan, Z. Gao, B. Shim, K. Yang, G. Mao, and M.-S. Alouini, "Compressive sensing based channel estimation for millimeter-wave full-dimensional MIMO with lens-array," *IEEE Trans. Veh. Technol.*, vol. 69, no. 2, pp. 2337–2342, Dec. 2020.
- [19] Z. Gao, L. Dai, S. Han, C.-L. I, Z. Wang, and L. Hanzo, "Compressive sensing techniques for next-generation wireless communications," *IEEE Wireless Commun.*, vol. 25, no. 3, pp. 144–153, Feb. 2018.
- [20] J. Sherman, "Properties of focused apertures in the Fresnel region," *IEEE Trans. Antennas Propag.*, vol. 10, no. 4, pp. 399–408, Jul. 1962.
- [21] G. L. A. Alkhateeb, O. El Ayach and R. W. Heath, "Channel estimation and hybrid precoding for millimeter wave cellular systems," *IEEE J. Sel. Topics Signal Process.*, vol. 8, no. 5, pp. 831–846, Oct. 2014.